Chinese Chemical Letters 35 (2024) 108912

Contents lists available at ScienceDirect

Chinese Chemical Letters

journal homepage: www.elsevier.com/locate/cclet

A lipid droplets-targetable fluorescent probe for polarity detection in cells of iron death, inflammation and fatty liver tissue

Xing Tian[a,1], Di Wu[b,1], Wanheng Wei[a], Guifu Dai[b,*], Zhanxian Li[a], Benhua Wang[c,*], Mingming Yu[a,*]

[a] Green Catalysis Center and College of Chemistry, Zhengzhou University, Zhengzhou 450001, China
[b] School of Life Sciences, Zhengzhou University, Zhengzhou 450001, China
[c] Shenzhen Research Institute of Central South University, Shenzhen 518057, China

ARTICLE INFO

Article history:
Received 2 June 2023
Revised 7 August 2023
Accepted 8 August 2023
Available online 9 August 2023

Keywords:
Lipid droplets
AIE
Polarity
Ferroptosis
Fatty liver

ABSTRACT

Abnormal accumulation and metabolism of lipid droplets can lead to a variety of diseases. Polarity, a key parameter of the microenvironment, is closely associated with many diseases and dysfunctions in the body. It is important to elucidate the relationship between the physiological activity of lipid droplets (LDs) and the polarity of the microenvironment. In this work, based on push-pull mechanism, a fluorescent probe (*E*)-3-(5-(4-(diphenylamino)phenyl)thiophen-2-yl)-1-(2-hydroxyphenyl)prop–2-en-1-one (PPTH) with aggregation-induced emission (AIE) properties for the detection of polarity changes in cells was synthesized. PPTH not only visualize intracellular polarity fluctuation of iron death and inflammation but also distinguish between normal and fatty liver tissue.

Lipid droplets (LDs) are organelles in which neutral lipids are stored [1,2] and are considered to be inert reservoirs for energy storage, playing an essential role in many aspects of cell metabolism and proliferation [3,4]. However, there are few reports on the excellent molecular fluorescent LDs probes [5,6]. Encouragingly, there is a considerable evidence that LDs are closely associated with many physiological processes [7,8], such as cell activation, apoptosis and protein-protein interactions [9–11]. Abnormal accumulation and metabolism of lipid droplets can result in a variety of diseases such as inflammation, liver cancer, Alzheimer's disease [12,13]. Therefore, accurate monitoring of the behavior of LDs *in vivo* is important for analyzing its biological mechanisms, understanding its biological metabolism and for early detection of cancer.

Polarity is a significant parameter in the human microenvironment, where activation of differentiation and immune responses, vectorial transport of molecules between cell layers, cell migration and local membrane growth can all lead to changes in cell polarity [14,15]. Abnormal changes in polarity in the biological microenvironment are closely associated with a number of diseases and are therefore of wide interest [16–19]. The physiological activity of LDs is related to the polarity of the microenvironment. If left unregulated, LDs can be toxic (lipotoxic) and induce cellular dysfunction and apoptosis [20]. Ferroptosis is a new model of regulated cell death (RCD) that is essentially caused by lipid peroxide-dependent iron accumulation, which affects the polarity of LDs [21]. Therefore, it is important to construct an effective and accurate method for detecting changes in intracellular polarity in real time.

Molecular fluorescent LDs probes, due to their many advantages, including the ability to test in real time and *in situ* as well as outstanding sensitivity, have been developed as a variety of prospective tools now [5,22–24]. However, most of these probes have insufficient specificity for LDs, their poor photostability, or their severe "self-absorption" due to small Stokes shifts and their complex synthesis processes limit their use for cellular imaging, and their inability to identify the microstructure of tissues hinders the further realization of their potential applications [25–27]. In 2001, Tang's group [28] discovered an unusual "aggregation-induced emission (AIE)" photophysical phenomenon in some propeller-like molecules and found that these AIEgens do not normally emit in solution, but emit strongly in the aggregated state [29,30]. In contrast, AIE properties make probes mitigate defects and significantly improve the photostability, resulting in long-term stable tracking of biological targets [31].

Common and classic synthetic strategies of polarity probes include electron-donating (D) units and electron-accepting (A) units combined by π-bridge, the expansion of π-conjugation,

* Corresponding authors.
E-mail addresses: daiguifu@zzu.edu.cn (G. Dai), benhuawang@csu.edu.cn (B. Wang), yumm@zzu.edu.cn (M. Yu).
[1] These authors contributed equally to this work.

https://doi.org/10.1016/j.cclet.2023.108912
1001-8417/

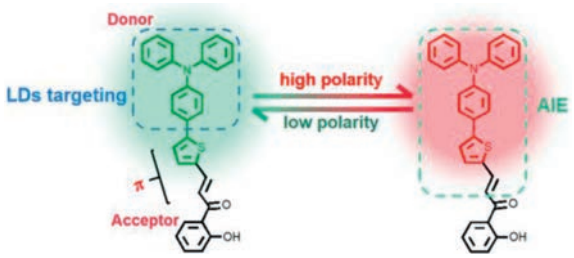

Scheme 1. Molecular structure of probe PPTH and the proposed polarity sensing mechanism.

or the merge of these two strategies, constructing a "D-π-A" structure. Moreover, the triphenylamine group has excellent AIE properties and is widely used in the exploitation of AIE fluorescent probes. For example, Tang's group [28] developed and readily prepared LDs-specific AIE fluorescent probes with good water-solubility, good biocompatibility and excellent membrane penetration based on triphenylamine derivatives for the first time [32,33]. Inspired by them, the fluorescent probe (*E*)−3-(5-(4-(diphenylamino)phenyl)thiophen-2-yl)−1-(2-hydroxyphenyl)prop–2-en-1-one (PPTH) with AIE properties was designed for the detection of polarity changes in lipid droplets based on push-pull mechanism, which is D-π-A type structured compound including a triphenylamine structural unit (working as D) and a thiophene segment (D and π-bridge), a π-bridge, and 2′-hydroxyacetophenone (A) (Scheme 1). This paper focuses on the AIE and polarity sensing properties of the probe PPTH and its application in bioimaging. Probe PPTH was simply prepared by a two-step reaction. The synthetic procedures for the probe PPTH were illustrated in Scheme S1 (Supporting information). PPTH also has the advantages of a large Stokes shift, high photostability, good selectivity to environmental polarity and low cytotoxicity. These features enable PPTH to visualize the formation and consumption of intracellular lipid droplets and to be used as a tool to detect changes in polarity within lipid droplets. It also enables the distinguishing between normal and fatty liver tissue.

At first, the photophysical properties of PPTH were detected in various polarity solvents by ultraviolet–visible (UV–vis) absorption and fluorescence spectra (Figs. S1 and S2 in Supporting information). Table S1 (Supporting information) summarizes the photophysical properties of PPTH. As presented in Fig. S1, UV–vis absorption spectra illustrated small changes for PPTH when the polarity of solvents increased from 1,4-dioxane to dimethyl sulfoxide (DMSO) and the maximum absorption wavelength was focused on 450 nm approximately. It shows that the dipole moment of the probe's ground state varies little with polarity. As illustrated in Fig. S2, with increasing polarity of these solvents, apparent red shift was observed in the fluorescence peaks of PPTH. Especially, great red shift from 549 nm (1,4-dioxane) to 633 nm (DMSO) was obtained in the maximum fluorescence emission wavelength of PPTH, giving Stokes shift of 101 nm and 171 nm, respectively. The fluorescence quantum yields of the probe PPTH in different solvents were investigated using fluorescein in 0.1 mol/L NaOH ($\varphi = 79\%$) as a standard (Table S1). The results show that the fluorescence quantum yield of the probe in DMSO ($\varphi = 1.62\%$) is much larger than that in 1,4-dioxane ($\varphi = 0.15\%$), and these phenomena indicate that the probe PPTH's dipole moment changes significantly in the excited state. This demonstrates the fluorescence properties of probe PPTH are extremely sensitive to the polarity of the solvent.

To gain more insight into the fluorescence response of PPTH to polarity and whether PPTH is AIE-active, the UV–vis spectra and fluorescence emission spectra of PPTH in the mixture of 1,4-dioxane (high solubility) and water (low solubility) were performed at 25 °C. Obviously, the absorption spectra changed very little (Fig. 1A). Surprisingly, PPTH is weakly emissive in 1,4-dioxane and the fluorescence rises with increasing water fraction gradually. This is accompanied by an obviously maximum emission wavelength redshift. This is contrary to the typical ICT effect phenomenon and may be under low polarity conditions (low water content), the probe PPTH emits a weak and short fluorescence due to its weak interaction with the solvent, where the molecules are dispersed. As the water (low solubility) content increases, the polarity of the solution is enhanced, and due to the interaction with the solvent, a large charge separation and the excited state energy dissipation may occur. Also in low solubility solvents, the restriction of intramolecular torsion caused by the aggregation of the probe in the solvent, AIE synergizes with polarity, resulting in strong and long fluorescence. Fluorescence spectra of PPTH (10 μmol/L) in 1,4-dioxane/H_2O mixture (0%–99% H_2O) and variation of maximum emission wavelength with water content were performed in Fig. S3 (Supporting information). Under excitation at 450 nm, in 1,4-dioxane, the fluorescence peak of 10 μmol/L PPTH was at 549 nm and gradually red-shifted to 644 nm with the water fraction in 1,4-dioxane/H_2O mixture increased from 0% to 15% and a Stokes shift of over 180 nm was obtained (Fig. 1B and Table S1), which may be suitable for eliminating potential interference from bioluminescence. Compared to that in 1,4-dioxane, the peak intensity (at 549 nm) of PPTH was increased by four times at $f_w = 15\%$. Notably, the fluorescence of probe PPTH has been red-shifted from yellow-green light area to the red light area when the water frac-

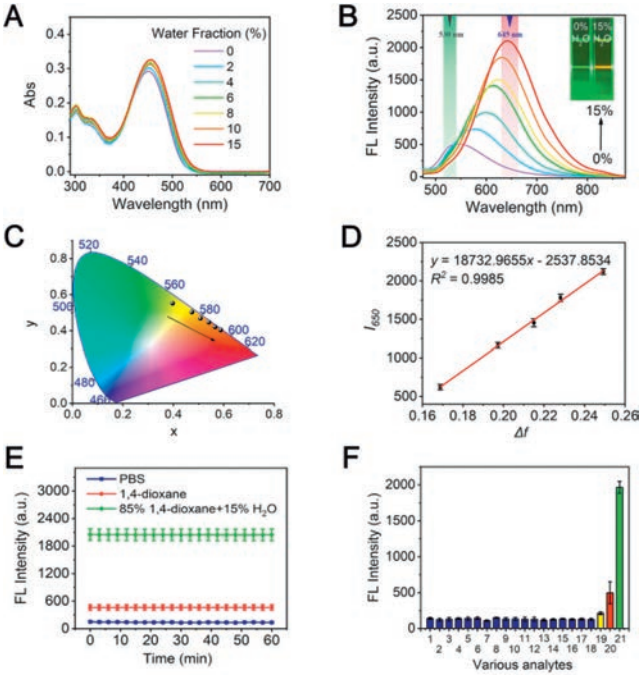

Fig. 1. UV–vis spectra (A) and fluorescence spectra (B) of PPTH (10 μmol/L) in 1,4-dioxane/H_2O mixture. $\lambda_{ex} = 450$ nm. Insert: photo of Tindal effect of PPTH under a laser pointer. (C) CIE1931 (x, y) color coordinates of 10 μmol/L PPTH in 1,4-dioxane/H_2O mixture. $\lambda_{ex} = 450$ nm. (D) Linearity between F_{max} and polarity Δf in the range from 0.17 to 0.25. (E) The time-dependent fluorescence changes of PPTH (10 μmol/L) in PBS buffer solvent (blue dash-dotted line), 1,4-dioxane solvent (red dash-dotted line), and in 85% 1,4-dioxane solvent (green dash-dotted line), respectively. $\lambda_{ex} = 450$ nm, slits: 10 nm, 5 nm. (F) Fluorescence intensity of PPTH (10 μmol/L) upon addition of different biologically relevants (2–18, 10 equiv.) and fluorescence intensity of PPTH (10 μmol/L) in different solvents (19–21), 1. blank, 2. L-glutathione (GSH), 3. Cys, 4. Hcy, 5. Glu, 6. Met, 7. HSO_3^-, 8. S^{2-}, 9. ClO^-, 10. H_2O_2, 11. SO_4^{2-}, 12. CO_3^{2-}, 13. Na^+, 14. Zn^{2+}, 15. K^+, 16. Fe^{2+}, 17. Fe^{3+}, 18. Ca^{2+}, 19. glycerol (yellow column), 20. 1,4-dioxane (red column), 21. 85% 1,4-dioxane + 15% H_2O (green column).

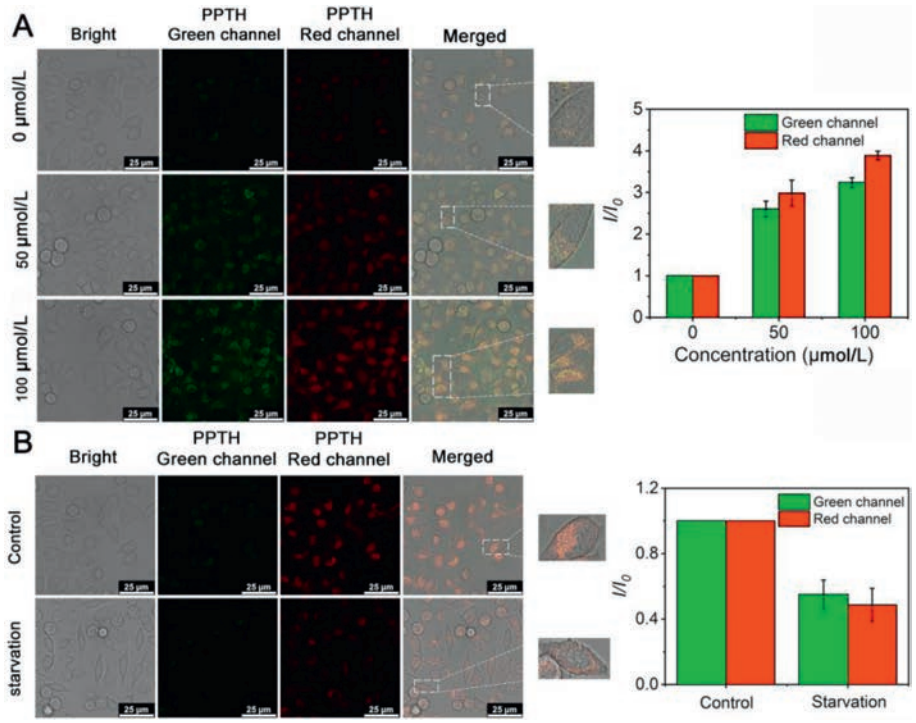

Fig. 2. (A) Fluorescence images of 10 μmol/L PPTH in HeLa cells pretreated with oleic acid of different concentration (0, 50, 100 μmol/L) and histogram of the relative pixel intensity of the fluorescence images (green channel: $\lambda_{ex} = 488$ nm, $\lambda_{em} = 520$–540 nm, red channel: $\lambda_{ex} = 488$ nm, $\lambda_{em} = 630$–660 nm). (B) Fluorescence images of 10 μmol/L PPTH in HeLa cells pretreated with PBS buffer solution for 2 h and histogram of the relative pixel intensity of the fluorescence images (green channel: $\lambda_{ex} = 488$ nm, $\lambda_{em} = 520$–540 nm, red channel: $\lambda_{ex} = 488$ nm, $\lambda_{em} = 630$–660 nm). Scale bar = 25 μm.

tion increased from 0% to 15% (Fig. 1C). In addition, at different polarities (in the mixed solvent of 1,4-dioxane and water), we performed a linear fit between the fluorescence intensity values of the probe at 650 nm and the solution polarizability (Δf). With increasing water content, the maximum emission wavelength of PPTH exhibited an excellent linear relationship with the polarizability of the solvent (Δf) in the area of solvent polarizability from 0.17 to 0.25 (Fig. 1D) ($R^2 = 0.9985$). These phenomena indicate a significant solvatochromic property of PPTH with increasing solvent polarity.

In addition, the quantum yield raised from 0.15 to 0.36 as the water fraction raised from 0% to 15%. It is believed that nanoaggregates are formed in 1,4-dioxane/H_2O mixture. Furthermore, under the light of the laser pointer, 10 μmol/L PPTH in 1,4-dioxane and 85% 1,4-dioxane (containing 15% water) all showed a Tindal effect, while that Tindal effect in the 85% 1,4-dioxane (including 15% water) was more obvious (Fig. 1B insert). Moreover, transmission electron microscopy (TEM) measurements were performed (Fig. S4 in Supporting information), the average particle size of probe PPTH in 85% 1,4-dioxane (containing 15% water) is significantly larger than the average particle size in 1,4-dioxane. The results of TEM further confirmed the aggregation of PPTH in 85% 1,4-dioxane (containing 15% water).

Photostability is an important factor affecting the bioimaging performance of the probe, and we assessed the photostability of the probe PPTH (Fig. 1E). The fluorescence intensity of the probe PPTH changed very little over 1 h under continuous irradiation with 450 nm excitation light in three different solvents. It shows that the probe PPTH has good photostability in both low and high polar environments.

The complexity of the cellular microenvironment in an organism, taking into account that the probe may be influenced by other biologically relevant substances in the organism when detecting polarity. We investigated the fluorescence intensity of phosphate buffer solution (PBS) buffer solvent when a variety of competing species co-existed with the probe PPTH (Fig. 1F). The results indicated that the fluorescence of the probe PPTH remained virtually unchanged compared with this probe in PBS solvent after the addition of various cations, anions, active sulfur (RSS) and reactive oxygen species (ROS), indicating that PPTH had good selectivity for polarity in complex multi-component biological systems.

In addition, the pH in an organism is a significant factor that interferes with probe polarity detection. Therefore, the UV–vis spectra and fluorescence emission spectra of the probe PPTH in acidic, neutral and basic environments was investigated. As displayed in Figs. S5 and S6 (Supporting information), the absorption spectra of the probe PPTH in 85% 1,4-dioxane + 15% H_2O mixture at pH 4, 7, 10 hardly changed and the fluorescence spectra changes very little under either acidic (pH 4) or alkaline (pH 10) conditions, suggesting that the detection properties of the probe PPTH are almost hardly disturbed by the acid-base environment and it was feasible to use probe PPTH to monitor polarity under the condition of physiological pH.

The size of the probe toxicity in the cells determines whether the probe can be used in biological experiments. Therefore, we measured the toxicity of the probe PPTH by cell counting kit-8 (CCK-8) assay before using the probe PPTH for cell imaging. The results are shown in Fig. S7 (Supporting information), PPTH is not cytotoxic in normal cells (hepatocyte L02) and the survival rate of HeLa cells was about 98%. Thus, PPTH exhibits negligible cytotoxicity in a certain concentration range, which can be further used for fluorescence imaging in organisms.

On the other hand, the photostability of the probe PPTH was assessed. HeLa cells were co-incubated with the probe PPTH, after which a time sequence was set and fluorescence images were recorded at 5 min intervals (Fig. S8A in Supporting information). The fluorescence images recorded in both the green and red channels displayed that the fluorescence of PPTH in HeLa cells did not change significantly within 30 min, which had good photostability in cells.

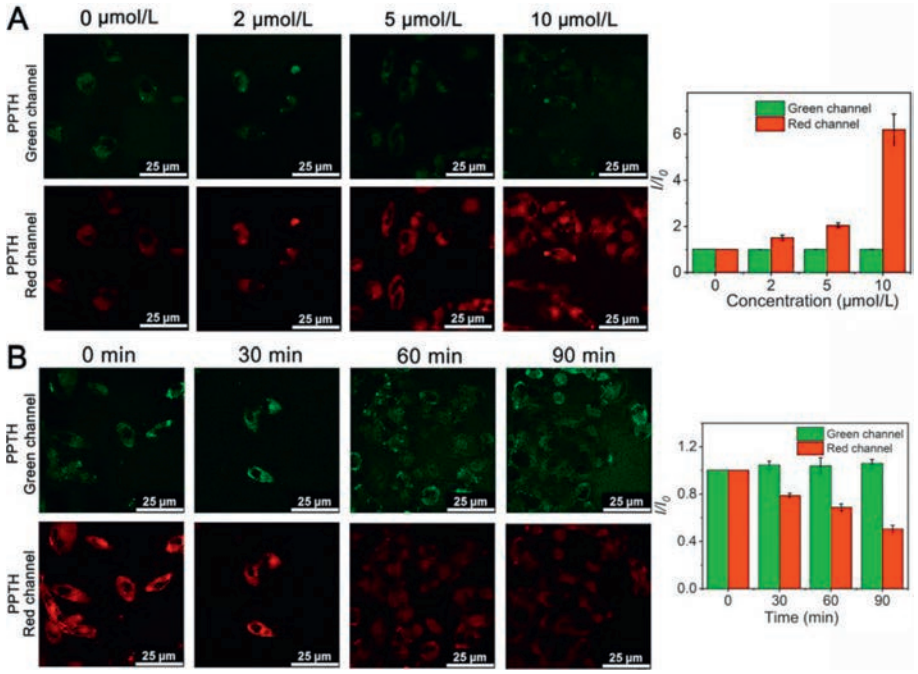

Fig. 3. (A) Fluorescence images of HeLa cells under ferroptosis induced by different concentration of RSL3 (0, 2, 5, 10 μmol/L) treated with 10 μmol/L PPTH. The histogram of the relative pixel intensity of the fluorescence images (Green channel: $\lambda_{ex} = 488$ nm, $\lambda_{em} = 520–540$ nm, red channel: $\lambda_{ex} = 488$ nm, $\lambda_{em} = 630–660$ nm). (B) Fluorescence images of HeLa cells treated with 50 μg/mL LPS and 10 μmol/L PPTH at different time points (0, 30, 60, 90 min). The histogram of the relative pixel intensity of the fluorescence images (Green channel: $\lambda_{ex} = 488$ nm, $\lambda_{em} = 520–540$ nm, red channel: $\lambda_{ex} = 488$ nm, $\lambda_{em} = 630–660$ nm). Scale bar = 25 μm.

Then, detailed cell-imaging experiments were conducted. To investigate whether the probe has the capacity to target lipid droplets, we investigated the ability of the probe PPTH to locate lipid droplets using a commercial dye for lipid droplets (LDs-Tracker Blue). The LDs-Tracker Blue was co-stained with the probe PPTH (10 μmol/L) for 5 h. Confocal images were taken to record the cell status. The images of the probe in the green and red channels overlap well with the commercial lipid dye in the blue channel, with co-localization coefficients of 0.94 and 0.92, respectively (Fig. S8B in supporting information). The result indicates that the probe PPTH has excellent lipid droplets targeting ability.

When the oleic acid is absorbed by cells, phase division occurs, which leads to a remarkable increase in neutral lipids in the cells [34]. The formation of lipid droplets in cells was simulated with oleic acid. It could be watched that the number of lipid droplets in the cytoplasm increased and the fluorescence intensity increased with the increase of oleic acid concentration (Fig. 2A). This phenomenon that more LDs were stained by fluorescence further indicated that PPTH could be selectively enriched on LDs. When the content of oleic acid reached 100 μmol/L, the relative fluorescence increased about four times compared to the initial one, indicating that PPTH could monitor LDs' accumulation. More interesting, when the living cells are deprived from nutrition in the early stage (starvation), they will be under pressure to survive, which will initiate related mechanisms to generate a great deal of energy materials in order to meet future survival requirements [9]. Thus, the starvation state will consume the lipids in the organism, causing a loss of lipids. We changed the culture medium of HeLa cells after staining with the probe PPTH (10 μmol/L) to PBS buffer solvent and continued to incubate for 2 h and then took pictures with the laser confocal instrument (Fig. 2B). The fluorescence intensity of green and red channels decreased, the number of red and green dots in merge images was significantly reduced, and the relative fluorescence intensity in starved cells decreased by about half, indicating a decrease in the number of lipid droplets. The above results demonstrate that the probe PPTH can visualize the formation and consumption of lipid droplets and will contribute to relevant biological studies.

On the basis of above results, the ferroptosis identification was further tested in live cells and the ability of the probe PPTH was evaluated to monitor changes in intracellular polarity. Ferroptosis is a caspase-independent cell death pathway identified in recent years, strongly associated with iron [35–37]. Drug-induced ferroptosis leads to an increase in the polarity of cells [38]. In the present work, RSL3 can induce the ferroptosis through covalently modifying the glutathione peroxidase 4 (GPX4) and inhibiting its activity, so we chose RSL3 as a tool to increase cell polarity. As shown in Fig. 3A, with increasing concentrations of RSL3, gradual decrease in the green channel and gradual increase in the red channel were observed, indicating the intracellular polarity gradually increase. It is clear from the graph that the relative fluorescence intensity has increased by a factor of approximately 6-fold. These results confirm that cell polarity exhibits a corresponding increase during RSL3-induced ferroptosis.

To investigate whether the probe PPTH can be applied in different physiological processes with changing polarity, we did the following studies. Inflammation is a precursor to the development of cancer and can lead to a decrease in polarity. Lipopolysaccharide (LPS), on the other hand, can cause cascading immune stimulation and toxic pathophysiological activity in the body and is therefore widely used to induce an inflammatory response in cells [39]. The HeLa cells were stained with PPTH (10 μmol/L) over time after induction by adding 50 μg/mL of LPS. As shown in Fig. 3B, it is obvious that the intracellular polarity starts to weaken over time, a weakly fluorescent increase in the green channel and a gradual decrease in the red channel were checked, suggesting that LPS-induced reduction in inflammatory cell polarity. The above cellular experimental results also demonstrate that the probe PPTH can be used as a fluorescent probe to detect changes in intracellular polarity.

Abnormal aggregation of LDs in tissues may result in fatty liver, which in turn may cause hepatic dysfunction [40,41]. It is there-

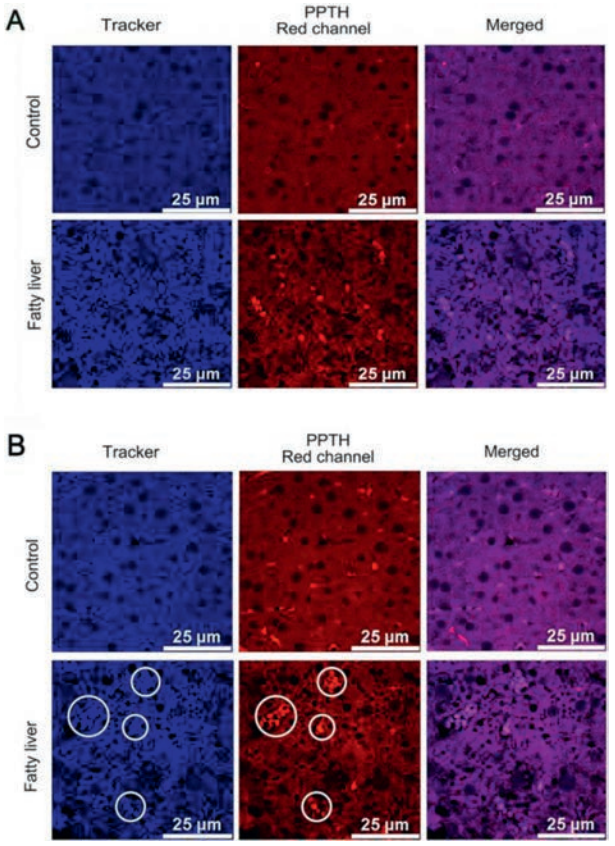

Fig. 4. (A) Colocalization imaging of the liver tissue from mice with normal mice and fatty liver stained using LDs-Tracker Blue (λ_{ex} = 408 nm, λ_{em} = 450–490 nm) and PPTH (λ_{ex} = 488 nm, λ_{em} = 590–680 nm). (B) Confocal fluorescence images of normal liver and fatty liver tissues of mice stained by LDs-Tracker Blue (λ_{ex} = 408 nm, λ_{em} = 450–490 nm) and PPTH (λ_{ex} = 488 nm, λ_{em} = 590–680 nm). The white circled areas are clusters of LDs formed in the liver tissue.

fore important to differentiate between areas of lipid and normal areas to prevent progression of the disease. For this purpose, a fatty liver mouse model has been established. Animal experiments were approved by the Experimental Animal Ethics Committee of the Zhengzhou University (No. ZZUIRB2022–03), and performed in accordance with the ethical guidelines of the Henan Province Experimental Animal Management Committee and the National Institutes of Health Guide for the Care and Use of Laboratory Animals. As shown in Fig. S9 (Supporting information), tissues from mice with fatty liver showed significant aggregation of LDs compared to controls, indicates the successful mouse model was established. Then, we discussed the potential ability of PPTH to target LDs in fatty liver tissue by staining with LDs-Tracker Blue. From Fig. 4A, it is seen that the PPTH overlaps well with the commercial dye-stained areas of the lipid droplets organelles, with a Pearson coefficient as high as 0.93, indicating that the probe PPTH has the ability to accurately localize lipid droplets in fatty liver tissue. Further, we evaluated the use of PPTH to distinguish between normal mouse liver tissue and fatty liver tissue (Fig. 4B). Compared to that in normal liver tissues, partial aggregation and significantly enhanced bright red fluorescence were observed, indicating more and a larger size of LDs could be significantly detected in fatty liver tissues. This result indicates that the probe PPTH has an excellent ability to distinguish between the lipid and normal regions.

To sum up, based on the dual mechanism of AIE and push-pull mechanism, we have synthesized a polar fluorescent probe PPTH to target lipid droplets. The probe PPTH shows a large Stokes shift (~180 nm) and is highly sensitive and selective to the polarity of the environment, with a gradual increase in fluorescence and red shift with increasing polarity. And the probe PPTH can visualize the formation and consumption of intracellular lipid droplets. By applying the process of ferroptosis and building cellular inflammation with LPS as a biological model, the probe PPTH can be used as a tool to detect changes in polarity within lipid droplets. It also enables the detection and visualization of fatty liver in small animals and effectively distinguishes between normal and fatty liver tissue.

Declaration of competing interest

The authors declare that they have no known competing financial interests or personal relationships that could have appeared to influence the work reported in this paper.

Acknowledgments

We are grateful for the financial supports from Scientific and Technological Key Project in Henan Province (No. 22170015), National Natural Science Foundation of China (No. U1704161), Zhengzhou University (No. 32211807) and Henan Provincial Science and Technology Research Project (No. JC21253010), Basic Research Foundation of Shenzhen Science and Technology Innovation (No. JCYJ20190806144605441).

Supplementary materials

Supplementary material associated with this article can be found, in the online version, at doi:10.1016/j.cclet.2023.108912.

References

[1] J. Yin, J. Zhan, Q. Hu, S. Huang, W. Lin, Chem. Soc. Rev. 52 (2023) 2011–2030.
[2] X. Zheng, W. Zhu, F. Ni, et al., Chem. Sci. 10 (2019) 2342–2348.
[3] D. Shi, L. Hu, X. Li, et al., Sens. Actuator. B: Chem. 319 (2020) 128302.
[4] J. Zheng, S. Qin, L. Gui, et al., Chin. Chem. Lett. 32 (2021) 2385–2389.
[5] T.K. Fam, A.S. Klymchenko, M. Collot, Materials 11 (2018) 1768.
[6] M. Collot, T.K. Fam, P. Ashokkumar, et al., J. Am. Chem. Soc. 140 (2018) 5401–5411.
[7] Y. Guo, T.C. Walther, M. Rao, et al., Nature 453 (2008) 657–661.
[8] Y. Miyanari, K. Atsuzawa, N. Usuda, et al., Nat. Cell. Biol. 9 (2007) 1089–1097.
[9] L. Yu, Y. Chen, S.A. Tooze, Autophagy 14 (2018) 207–215.
[10] J. Boren, K.M. Brindle, Cell Death Differ. 19 (2012) 1561–1570.
[11] L. Fan, X. Wang, Q. Zan, Anal. Chem. 93 (2021) 8019–8026.
[12] N. Krahmer, R.V. Farese Jr, T.C. Walther, EMBO. Mol. Med. 5 (2013) 973–983.
[13] H. Zhu, K. Ma, R. Ruan, et al., Chin. Chem. Lett. 35 (2024) 108536.
[14] J. Hu, Y. Sun, X. Geng, et al., Light Sci. Appl. 11 (2022) 185.
[15] J. Cui, Y. Yao, C. Chen, et al., Chin. Chem. Lett. 30 (2019) 1071–1074.
[16] N. Jiang, J. Fan, F. Xu, et al., Angew. Chem. Int. Ed. 54 (2015) 2510–2514.
[17] T. Yang, Y. Zuo, Y. Zhang, et al., Anal. Chim. Acta 1091 (2019) 88–94.
[18] M. Li, J. Fan, H. Li, et al., Biomaterials 164 (2018) 98–105.
[19] T. Zhao, F. Huo, W. Zhang, et al., Chem. Eng. J. 437 (2022) 135397.
[20] H. Tian, A.C. Sedgwick, H.H. Han, et al., Coordin. Chem. Rev. 427 (2021) 213577.
[21] B. Zhai, W. Hu, S. Zhai, et al., Talanta 256 (2023) 124304.
[22] P. Tan, W. Zhuang, S. Li, et al., Chem. Commun. 57 (2021) 1046–1049.
[23] S. Li, W. Zhuang, J. Chen, et al., J. Mater. Chem. B 9 (2021) 4050–4055.
[24] G. Liu, G. Peng, J. Dai, et al., Anal. Chem. 93 (2021) 14784–14791.
[25] D. Dang, H. Liu, J. Wang, et al., Chem. Mater. 30 (2018) 7892–7901.
[26] Y. Xu, C. Li, J. An, et al., Sci. China Chem. 66 (2022) 155–163.
[27] M. Jiang, X. Gu, J.W.Y. Lam, et al., Chem. Sci. 8 (2017) 5440–5446.
[28] J. Luo, Z. Xie, J.W. Lam, et al., Chem. Commun. (2001) 1740–1741.
[29] J. Mei, N.L.C. Leung, R.T.K. Kwok, et al., Chem. Rev. 115 (2015) 11718–11940.
[30] X. Wang, S. Chen, Y. Jia, et al., Chin. Chem. Lett. 34 (2023) 107866.
[31] J. Zhang, B. Xu, W. Tian, et al., Chem. Sci. 9 (2018) 2620–2627.
[32] P. Ning, W. Wang, M. Chen, et al., Chin. Chem. Lett. 28 (2017) 1943–1951.
[33] D. Wang, H. Su, R.T.K. Kwok, et al., Chem. Sci. 9 (2018) 3685–3693.
[34] K. Wang, S. Ma, Y. Ma, et al., Anal. Chem. 92 (2020) 6631–6636.
[35] L. Jiang, N. Kon, T. Li, et al., Nature 520 (2015) 57–62.
[36] H. Yu, P. Guo, X. Xie, et al., J. Cell. Mol. Med. 21 (2017) 648–657.
[37] W.S. Yang, R. SriRamaratnam, M.E. Welsch, et al., Cell 156 (2014) 317–331.
[38] K.N. Wang, L.Y. Liu, D. Mao, et al., Angew. Chem. Int. Ed. 60 (2021) 15095–15100.
[39] R. Li, J. Guo, Y. Duan, et al., Chem. Eng. J. 435 (2022) 135043.
[40] N.L. Gluchowski, M. Becuwe, T.C. Walther, R.V. Farese, Nat. Rev. Gastro. Hepat. 14 (2017) 343–355.
[41] H. Song, W. Zhang, Y. Zhang, et al., Chem. Eng. J. 445 (2022) 136448.